

SCIENTIFIC REPORTS

Corrected: Author Correction

OPEN

Radiological Investigation of High Background Radiation Areas

Fawzia Mubarak¹, M. Fayez-Hassan², N. A. Mansour³, Talaat Salah Ahmed¹ & Abdallah Ali¹

In this paper, we used the Hyper-Pure Germanium (HPGe) detector to measure 30 samples which are collected from north of Nile Delta near Rosetta beach in Egypt. The activity of primordial radionuclides, such as ^{238}U , ^{235}U , ^{232}Th , and ^{40}K was estimated. Concentrations ranged between 36.5–177.4, 50–397.5 and 56.1–168.9 Bq.kg⁻¹ for ^{238}U , ^{232}Th and ^{40}K respectively. Activity concentration of ^{235}U and the variation in uranium isotopic ratio $^{235}\text{U}/^{238}\text{U}$ was calculated. External hazard indices (H_{ex}) (or radium equivalent activity Ra_{eq}), activity concentration indices (I), alpha index (I_{α}), absorbed outdoor gamma dose rate (D_{out}), effective outdoor gamma dose rate (E_{out}) and Excess Lifetime Cancer Risk (ELCR) due to different samples are estimated. External hazard indices (H_{ex}) are ranged between 0.32–2.04, radium equivalent activity (Ra_{eq}) are ranged between 118.67–753.91, the activity concentration indices (I) are 0.42–2.61, and alpha index (I_{α}) are 0.18–0.89. External hazard indices (H_{ex}) in some samples more than unity then it exceeds the upper limit of exposure. Also, the radium equivalent activities (Ra_{eq}) are higher than the exemption limits (370 Bq.kg⁻¹).

Human beings always are exposed to natural radiation, which is mainly due to the activity of natural radionuclides: ^{238}U (^{226}Ra) series, ^{232}Th series and ^{40}K that are present in the earth's crust, in building materials, air, water, food and the human body. Naturally occurring radionuclides in soils are the major contributors of outdoor terrestrial natural radiation¹. Due to these radionuclides are not uniformly distributed, the understanding of their distribution in soil, sand, and rock are very important in radiation protection and measurement². The associated external exposures due to gamma radiation emitted from these radionuclides depend on the geographical and geological conditions and were varied vary from region to another in the world. High background radiation areas, (HBRAs) are distributed through some regions in the world³. In Egypt, there are some areas known for their HBRAs whose geological and geochemical characteristics increase the levels of natural radiation. Black sand one of the most famous materials that have high background radiation and it contributes to increasing the environmental dose⁴. Beach sands are mostly composed of feldspar, quartz and other minerals opposing to wave abrasion. They are formed due to fragmentation, weathering, and degradation. Beach placer or “black sand” deposits around Mediterranean Sea beaches are known for their economic concentrations of different minerals such as Monazite, Zircon, Biotite, Rutile, Chromite, Garnet, Allanite and Sillimanite, Tourmaline, Sphene, Pyroxenes, Haematite, Ilmenite, Niobian-Rutile, and Pyrrhotite. Pyrrhotite and Niobian-Rutile were found in magnetite and Ilmenite respectively^{5,6}. Hinterland geology, sub-tropical climate, geomorphology and intricate network drainage aided by wind, waves, and currents have influenced these formations. Monazite bearing black sands contains ^{232}Th with some extent of ^{238}U and ^{40}K ^{7,8}. The main activity of the uranium and thorium series is due to the fractions of zircon, Ilmenite and little of it due to garnet ^{238}U activity was controlled by heavy non-magnetic (HNM) fraction (Monazite, Zircon, Titanite and Apatite), while the heavy magnetic (HM) fraction, at least for the heavy mineral rich samples bearing high amounts of Epidote crystals with Allanite cores, control their ^{232}Th content^{9–11}. Studies concerning the radiation risks arising from exposure to black sand showed that is the main source of external dose to the world population was due to natural radiation^{12–14}.

This study investigates the distribution of natural radionuclides in the north of Nile Delta near Rosetta beach to understand the radiological risks due to the gamma-ray exposure¹⁵. Samples were collected from east to west and locations were divided into 12 groups, spaced in-between by about 600 m and extending into the land from the beach line for about 50 m or less, Fig. (1).

¹Radiation Protection Dept., Nuclear Research Center, Egyptian Atomic Energy Authority, Cairo, Egypt.

²Experimental Nuclear Physics Dept., Nuclear Research Center, Egyptian Atomic Energy Authority, Cairo, Egypt.

³Faculty of Science, Zagazig University, El-Sharkia, Egypt. Correspondence and requests for materials should be addressed to A.A. (email: Abdallah.ph999@yahoo.com)

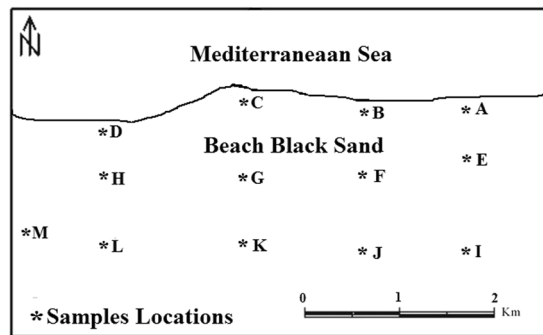


Figure 1. Sampling locations.

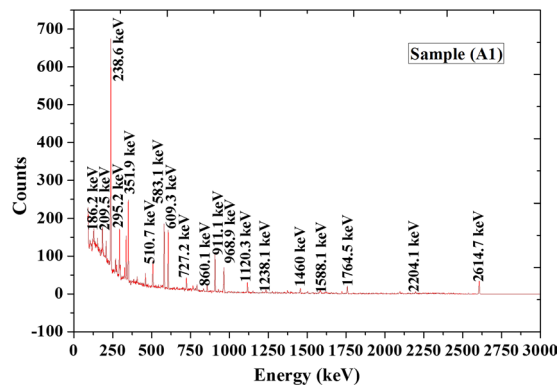


Figure 2. Spectrum analysis for sample (A1).

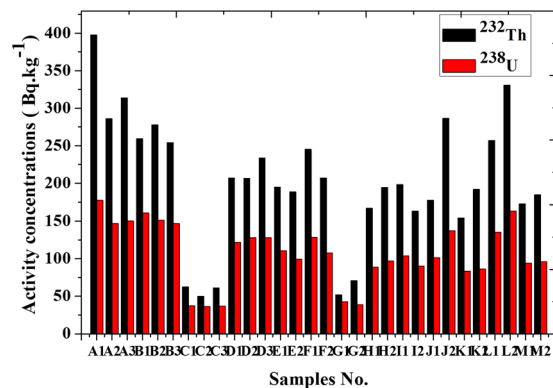


Figure 3. Activity concentrations of ^{232}Th and ^{238}U (Bq.kg^{-1}) for different samples.

Results

Figure (2) shows an example of spectrum analysis of black sand beach. Samples are dominated by Th and U-bearing minerals due to the presence of significant amounts of Monazites and Zircon as shown in Fig. (3).

Table (1) shows activity concentration (Bq.kg^{-1}) of different samples. They were ranged between 36.5–177.4 with an average of 107.6 Bq.kg^{-1} for ^{238}U , 50–397.5 with an average of 201.6 Bq.kg^{-1} for ^{232}Th and 56.1–168.9 with an average of 116.2 Bq.kg^{-1} for ^{40}K .

The specific activities ratio ($^{232}\text{Th}/^{238}\text{U}$) in sand samples varied from 1.22 to 2.24 with a mean value of 1.84 this is due to that Monazite contains more thorium than uranium¹⁶. A correlation exists between the activity of ^{232}Th and ^{238}U in black sand beach samples ($R^2 = 0.94$) with fitting equation $^{232}\text{Th} = 2.17 \times ^{238}\text{U} - 20.71$ and standard error (± 4.7) as shown in Fig. (4).

Figure (5) illustrates the relation between $^{226}\text{Ra}_{\text{eq}}$ and ^{238}U activity with the fitted straight line ($R^2 = 0.96$). This indicated a positive and strong correlation coefficient between uranium concentration and radium equivalent activity level in black sand beach samples.

Sample	Activity Concentration (Bq.kg ⁻¹) ²³⁸ U ²³² Th ⁴⁰ K ²³⁵ U				²³⁵ U/ ²³⁸ U ratio
A1	177.4 ± 39.7	397.5 ± 71.5	105.0 ± 15.8	9.8 ± 8	0.055
A2	146.9 ± 26.6	286.0 ± 12.0	93.0 ± 10.7	7.3 ± 0.5	0.049
A3	150.4 ± 42.9	313.9 ± 12.1	103.0 ± 13.5	6.3 ± 0.4	0.042
B1	160.9 ± 63.9	259.4 ± 50.9	168.9 ± 17.5	11.1 ± 0.9	0.069
B2	151.4 ± 40.7	278.1 ± 36.1	83.5 ± 11.3	9 ± 0.8	0.059
B3	146.7 ± 21.0	254.2 ± 41.0	110.4 ± 12.7	6.6 ± 0.5	0.045
C1	37.6 ± 4.9	62.5 ± 18.3	151.1 ± 14.9	4 ± 0.5	0.106
C2	36.5 ± 7.0	50.0 ± 7.8	138.6 ± 19	2 ± 0.3	0.055
C3	36.6 ± 7.2	61.0 ± 13.8	144.8 ± 17.5	2.5 ± 0.2	0.068
D1	121.6 ± 26.9	207.3 ± 44.6	94.8 ± 11.5	11 ± 0.8	0.090
D2	128.0 ± 28.1	206.7 ± 20.2	117.6 ± 13.4	5.7 ± 0.6	0.045
D3	128.3 ± 36.2	233.7 ± 51.0	89.4 ± 14.3	9.4 ± 0.8	0.073
E1	110.6 ± 22.7	194.8 ± 24.4	91.8 ± 12.6	6.7 ± 0.7	0.061
E2	99.3 ± 19.8	188.5 ± 32.6	129.9 ± 18.2	5.2 ± 0.5	0.052
F1	128.8 ± 19.0	245.2 ± 36.8	76.0 ± 9.8	10.6 ± 0.9	0.082
F2	107.5 ± 23.5	207.1 ± 34.9	118.0 ± 12.7	7.8 ± 0.7	0.073
G1	42.7 ± 5.4	52.2 ± 13.5	150.0 ± 14.6	3.1 ± 0.2	0.073
G2	39.1 ± 21.4	70.9 ± 5.2	134.1 ± 14.2	3.8 ± 0.2	0.097
H1	88.7 ± 13.7	167.1 ± 39.7	92.9 ± 8.5	5.1 ± 0.4	0.057
H2	96.9 ± 22.7	194.6 ± 13.7	107.5 ± 9.2	11.1 ± 0.9	0.115
I1	103.6 ± 33.5	198.4 ± 32.2	133.8 ± 12.6	3.1 ± 0.2	0.030
I2	90.4 ± 32.0	163.4 ± 38.9	142.2 ± 12.8	6.8 ± 0.5	0.075
J1	101.5 ± 31.8	177.6 ± 21.2	130.5 ± 11.6	5.8 ± 0.4	0.057
J2	137.4 ± 35.6	286.6 ± 61.9	130.7 ± 13.1	10.4 ± 0.8	0.076
K1	83.4 ± 21.6	154.5 ± 25.0	110.1 ± 8.8	2.5 ± 0.2	0.030
K2	86.4 ± 13.8	192.2 ± 9.7	107.5 ± 7.6	5.7 ± 0.3	0.066
L1	135.2 ± 35.7	257.1 ± 47.9	131.8 ± 11.5	7.6 ± 0.7	0.056
L2	163.3 ± 28.1	330.9 ± 65.5	122.8 ± 10.3	10.8 ± 0.9	0.066
M1	93.9 ± 12.5	172.5 ± 34.2	56.1 ± 5.8	8.2 ± 0.6	0.087
M2	95.9 ± 31.3	184.8 ± 30.2	120.5 ± 11.9	2.5 ± 0.4	0.026
Min	36.6 ± 7.2	50.0 ± 7.8	56.1 ± 5.8	2 ± 0.3	0.026
Max	177.4 ± 39.7	397.5 ± 71.5	168.9 ± 17.5	11.1 ± 0.9	0.115
Average ± St. Dev.	107.6 ± 40.2	201.6 ± 84.8	116.2 ± 25.2	6.86 ± 2.9	0.065 ± 0.021

Table 1. Activity concentration of different samples at different locations and ²³⁵U/²³⁸U ratio.

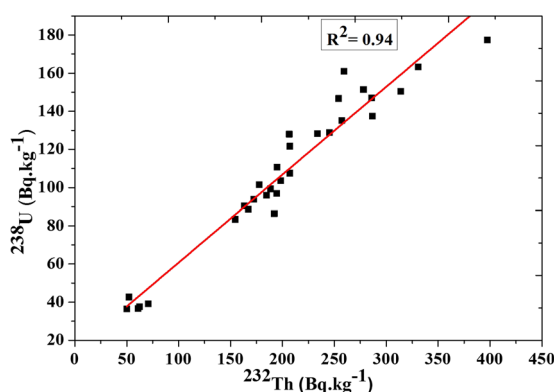


Figure 4. Correlation between the activity concentrations for ²³²Th and ²³⁸U.

Activity concentration of ²³⁵U and the variation in uranium isotopic ratio ²³⁵U/²³⁸U also is shown in the Table (1). The specific activities ratio (²³⁵U/²³⁸U) in black sand beach samples varied from 0.026 to 0.115 with an average value of 0.065. A correlation exists between ²³⁵U and ²³⁸U in black sand beach samples ($R^2 = 0.51$) with fitting equation $^{235}\text{U} = ^{238}\text{U}/9.9 - 4.15$ and standard error (± 1.1) as shown in Fig. (6). Figure (7) shows an example for U-235 concentration spectrum.

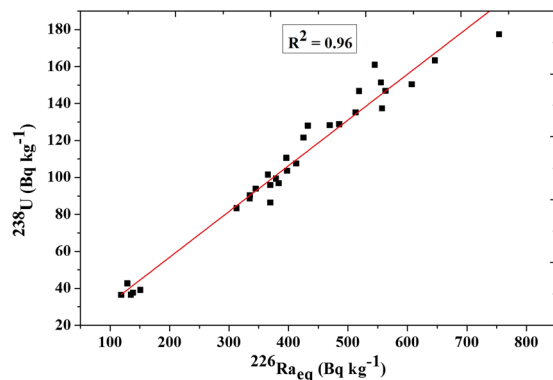


Figure 5. Correlation between the activity concentrations for ^{238}U and $^{226}\text{Ra}_{\text{eq}}$.

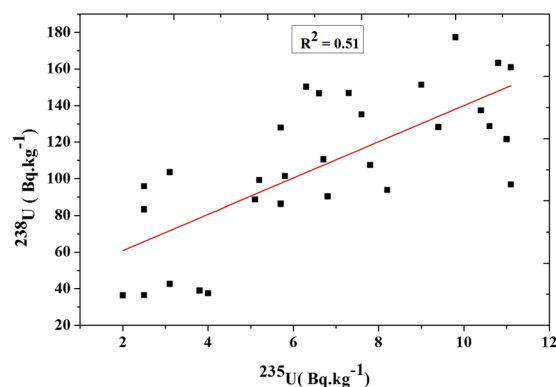


Figure 6. Correlation between the activity concentrations for ^{235}U and ^{238}U .

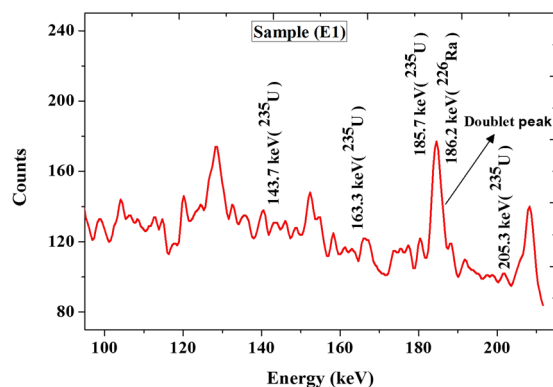


Figure 7. Spectrum of ^{235}U Gamma ray energies and doublet peak of ^{235}U (185.7 keV) plus ^{226}Ra (186.2 keV) for sample (E1).

The frequency distribution and the cumulative probability of different isotopes (^{238}U , ^{235}U , ^{232}Th and ^{40}K) for different samples are shown in Fig. (8).

Table (2) shows external hazard indices (H_{ex}), activity concentration indices (I), radium equivalent activity (Ra_{eq}), alpha index (I_{α}), absorbed outdoor gamma dose rate (D_{out}) and effective outdoor gamma dose rate (E_{out}) due to different samples. External hazard indices (H_{ex}) were ranged between 0.32 and 2.04, radium equivalent activity (Ra_{eq}) were ranged between 118.67 to 753.91, activity concentration indices (I) were 0.42–2.61, and alpha index (I_{α}) were 0.18 to 0.89.

These results show that some locations lead to over-exposure, for example, external hazard indices (H_{ex}) in some samples are found to be more than unity then it exceeds the upper limit of exposure, Fig. (9). Also, radium equivalent activity (Ra_{eq}), Fig. (10), was higher than the exemption limits (370 Bq kg^{-1}) that keep the external dose below 1.5 mSv yr^{-1} as reported by UNSCEAR (2010)¹⁷. While activity concentration indices (I) slightly exceed

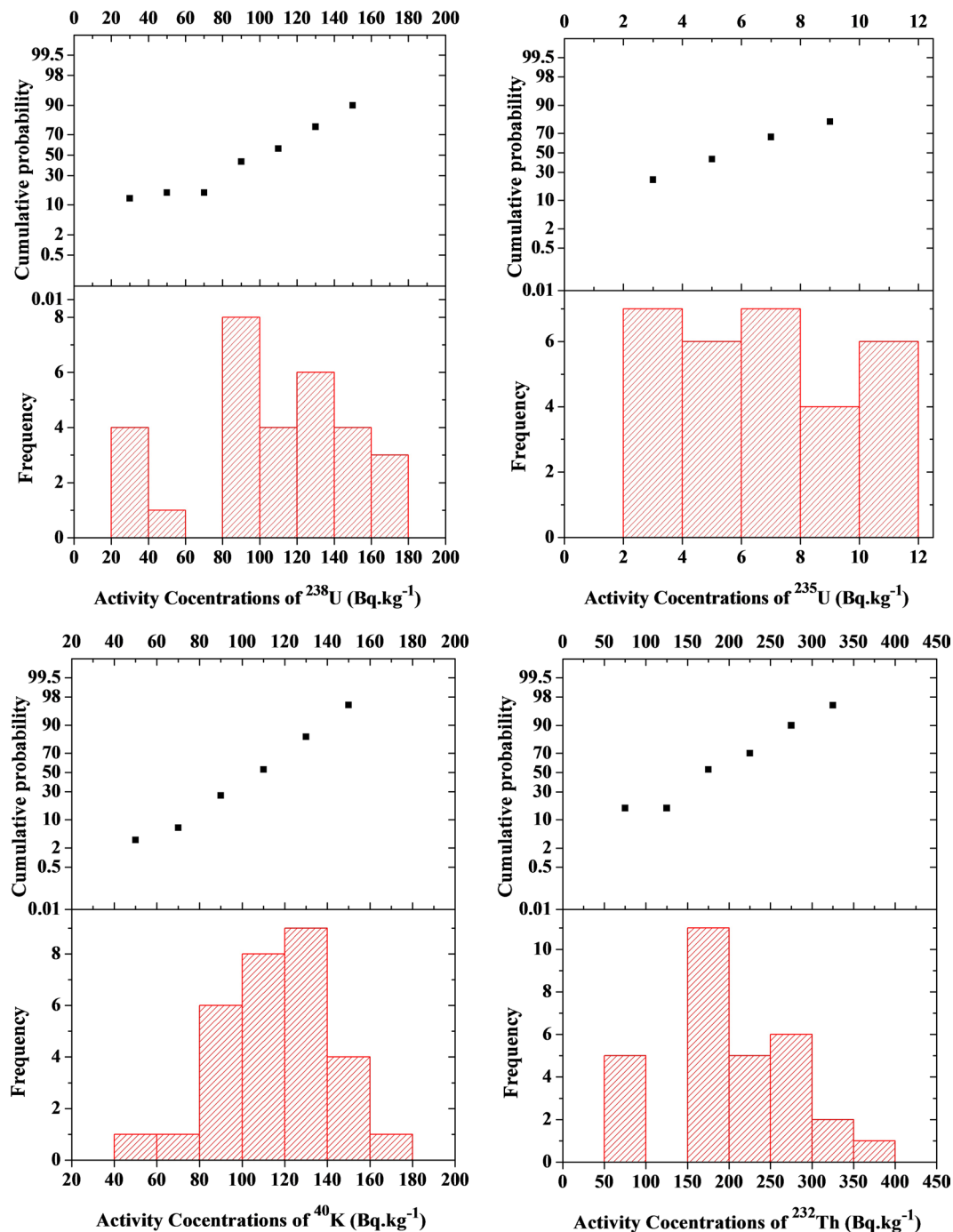


Figure 8. Histogram and cumulative probability plots for the frequency distribution of ²³⁸U, ²³⁵U, ²³²Th and ⁴⁰K for different samples.

the permissible limits which met 0.3 mSvyr^{-1} as shown in Fig. (11). Outdoor Excessive Lifetime Cancer Risk (ELCR_{out}) is found to be ranged between $0.24\text{E-}3$ – $1.49\text{E-}3$ with an average of $0.8\text{E-}3$ which is 2.8 times more than the upper limits $0.29\text{E-}3$ ¹⁸.

Figure (12) shows the outdoor absorbed gamma dose rate (D_{out}). It was ranged between 55.51 to 345.95 with an average of 186 nGy.h^{-1} which leads to effective outdoor gamma dose rate (E_{out}) ranged between 0.07 to 0.42 with an average of 0.23 mSvyr^{-1} which represented more than 3 times higher than the world's average of 0.07 mSv.yr^{-1} . The outdoor absorbed gamma dose rate was within the range as reported by UNSCEAR-2010 to Nile Delta region which met 20 – 400 nGy.h^{-1} as shown in the Table (3) in which a comparison between some high background radiation areas among the world was reported.

Table (4) shows total annual equivalent dose to different organs and effective dose due to exposure to the average value of the activity of all naturally occurring radionuclides (mSvyr^{-1}) in black sand.

Sample	Ra _{eq}	Hex	I	I _α	D _{out}	E _{out}	ELCR _{out} × 10 ⁻³
A1	753.91	2.04	2.61	0.89	345.95	0.42	1.49
A2	563.04	1.52	1.95	0.73	258.01	0.32	1.1
A3	607.21	1.64	2.11	0.75	278.57	0.34	1.20
B1	544.85	1.47	1.89	0.80	249.89	0.31	1.07
B2	555.51	1.50	1.92	0.76	254.24	0.31	1.09
B3	518.71	1.40	1.80	0.73	237.57	0.29	1.02
C1	138.61	0.37	0.49	0.19	64.89	0.08	0.28
C2	118.67	0.32	0.42	0.18	55.51	0.07	0.24
C3	134.98	0.36	0.48	0.18	63.17	0.08	0.27
D1	425.34	1.15	1.47	0.61	194.81	0.24	0.84
D2	432.64	1.17	1.50	0.64	198.23	0.24	0.85
D3	469.37	1.27	1.63	0.64	215.02	0.26	0.92
E1	396.23	1.07	1.37	0.55	181.61	0.22	0.78
E2	378.86	1.02	1.32	0.50	174.35	0.21	0.75
F1	485.29	1.31	1.68	0.64	222.26	0.27	0.95
F2	412.74	1.11	1.43	0.54	189.70	0.23	0.81
G1	128.90	0.35	0.45	0.21	60.18	0.07	0.26
G2	150.81	0.41	0.53	0.20	70.34	0.09	0.30
H1	334.81	0.90	1.16	0.44	153.80	0.19	0.66
H2	383.46	1.04	1.33	0.48	176.32	0.22	0.76
I1	397.61	1.07	1.38	0.52	182.97	0.22	0.79
I2	335.01	0.90	1.17	0.45	154.38	0.19	0.66
J1	365.52	0.99	1.27	0.51	168.06	0.21	0.72
J2	557.30	1.51	1.93	0.69	256.10	0.31	1.10
K1	312.81	0.84	1.09	0.42	143.93	0.18	0.62
K2	369.52	1.00	1.28	0.43	170.21	0.21	0.73
L1	513.00	1.39	1.78	0.68	235.56	0.29	1.01
L2	645.94	1.74	2.24	0.82	296.37	0.36	1.27
M1	344.89	0.93	1.19	0.47	157.90	0.19	0.68
M2	369.44	1.00	1.28	0.48	169.98	0.21	0.73
Min.	118.67	0.32	0.42	0.18	55.51	0.07	0.24
Max.	753.91	2.04	2.61	0.89	345.95	0.42	1.49
Av. ± Stdev	1.1 ± 0.4	404.8 ± 159.9	1.4 ± 0.6	0.54 ± 0.2	186. ± 73	0.2 ± 0.1	0.8 ± 0.3

Table 2. External hazard indices (H_{ex}), radium equivalent Ra_{eq}, activity concentration indices (I), alpha index I_α, absorbed dose (D_{out}), effective (E_{out}) outdoor gamma dose rate and Excessive Lifetime Cancer Risk (ELCR_{out}) due to different samples.

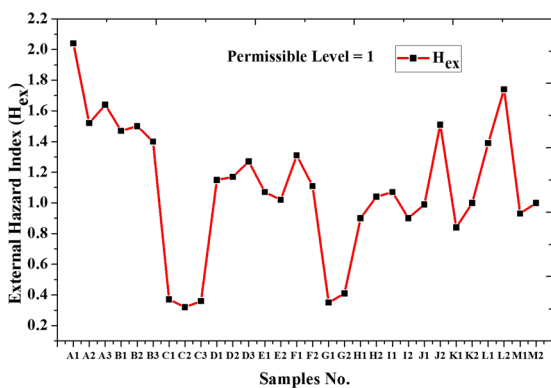


Figure 9. External Hazard Index (H_{ex}) for different samples.

Figure (13) investigate the annual equivalent dose to different organs due to the average value of activity concentrations of all-natural radionuclides it was ranged between 6.28E-4 (received by the pancreas) and 1.35E-3 mSv.yr⁻¹ (received by skin).

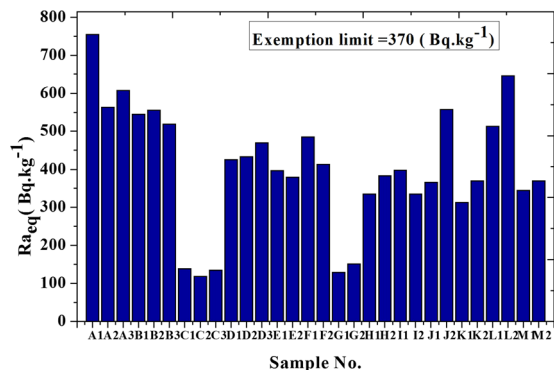


Figure 10. Radium equivalent for different samples.

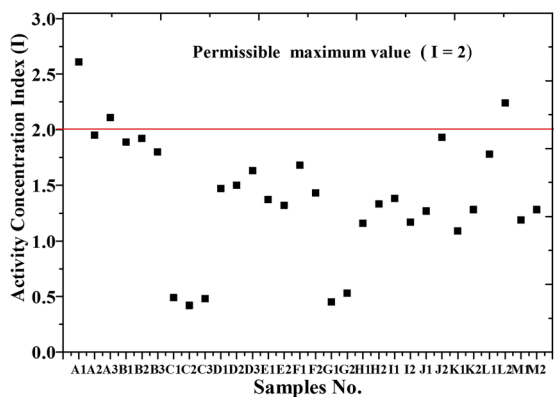


Figure 11. Activity concentration indices for different samples.

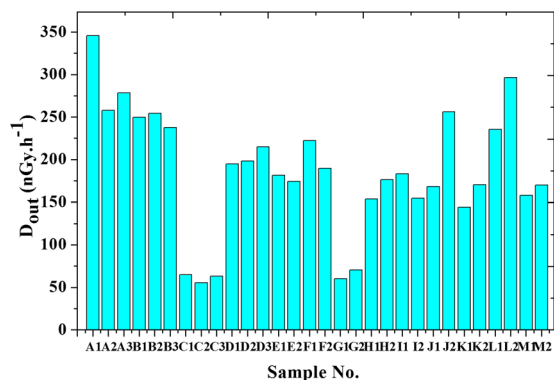


Figure 12. Outdoor absorbed dose for different samples.

Country	Area	Area Characteristics	Absorbed dose rate in air (nGy.h ⁻¹)
Brazil	Guarapari	Monazite sands; coastal areas	90–170 (streets) 90–90000 (beaches) 110–1 300
China	Yangjiang Quangdong	Monazite particles	370 average
India	Kerala Ganges Delta	Monazite sands,	200–4000 1800 average 260–440
Egypt	Nile Delta	Monazite sands	20–400
Present study	North of Nile Delta	Monazite sands	55.51–345.95 186 average

Table 3. A comparison of our study with other studies of black sand beaches²².

Organ	^{238}U	^{232}Th	^{40}K	Summation
R Marrow	3.33×10^{-8}	5.81×10^{-7}	6.87×10^{-4}	6.87×10^{-4}
Adrenals	2.31×10^{-8}	5.07×10^{-7}	7.82×10^{-4}	7.83×10^{-4}
B Surface	2.02×10^{-7}	2.43×10^{-6}	7.00×10^{-4}	7.02×10^{-4}
Brain	2.61×10^{-8}	5.90×10^{-7}	6.90×10^{-4}	6.90×10^{-4}
Breast	1.62×10^{-7}	9.62×10^{-7}	6.72×10^{-4}	6.73×10^{-4}
G Bladder	2.21×10^{-8}	5.01×10^{-7}	6.32×10^{-4}	6.33×10^{-4}
Esophagus	1.60×10^{-8}	4.44×10^{-7}	7.39×10^{-4}	7.40×10^{-4}
ST Wall	2.99×10^{-8}	5.87×10^{-7}	7.34×10^{-4}	7.35×10^{-4}
SI Wall	2.03×10^{-8}	4.90×10^{-7}	7.26×10^{-4}	7.27×10^{-4}
ULI Wall	2.29×10^{-8}	5.21×10^{-7}	6.52×10^{-4}	6.52×10^{-4}
LLI Wall	2.17×10^{-8}	5.10×10^{-7}	6.55×10^{-4}	6.56×10^{-4}
Heart	2.73×10^{-8}	5.64×10^{-7}	6.67×10^{-4}	6.67×10^{-4}
Kidneys	3.54×10^{-8}	6.07×10^{-7}	6.85×10^{-4}	6.86×10^{-4}
Liver	3.01×10^{-8}	5.98×10^{-7}	6.80×10^{-4}	6.81×10^{-4}
Lungs	3.57×10^{-8}	6.73×10^{-7}	7.31×10^{-4}	7.32×10^{-4}
Ovaries	1.99×10^{-8}	4.72×10^{-7}	6.49×10^{-4}	6.49×10^{-4}
Pancreas	1.86×10^{-8}	4.78×10^{-7}	6.27×10^{-4}	6.28×10^{-4}
Skin	5.42×10^{-7}	1.59×10^{-6}	1.35×10^{-3}	1.35×10^{-3}
Spleen	2.93×10^{-8}	5.98×10^{-7}	6.87×10^{-4}	6.87×10^{-4}
Testes	1.25×10^{-7}	8.76×10^{-7}	7.82×10^{-4}	7.83×10^{-4}
Thymus	3.62×10^{-8}	6.41×10^{-7}	7.00×10^{-4}	7.00×10^{-4}
Thyroid	4.45×10^{-8}	6.44×10^{-7}	6.90×10^{-4}	6.91×10^{-4}
U Bladder	2.90×10^{-8}	5.67×10^{-7}	6.72×10^{-4}	6.72×10^{-4}
Uterus	1.92×10^{-8}	4.78×10^{-7}	6.32×10^{-4}	6.33×10^{-4}
Muscle	8.65×10^{-8}	7.39×10^{-7}	7.39×10^{-4}	7.40×10^{-4}
h_rem	8.07×10^{-8}	7.22×10^{-7}	7.34×10^{-4}	7.35×10^{-4}
E	6.51×10^{-8}	6.93×10^{-7}	7.26×10^{-4}	7.27×10^{-4}
Min	1.60×10^{-8} (Esophagus)	4.44×10^{-7} (Esophagus)	6.27×10^{-4} (Pancreas)	6.28×10^{-4} (Pancreas)
Max	5.42×10^{-7} (Skin)	2.43×10^{-6} (B-Surface)	1.35×10^{-3} (Skin)	1.35×10^{-3} (Skin)

Table 4. Annual equivalent dose and effective dose due to average activity ($\text{mSv}\cdot\text{yr}^{-1}$).

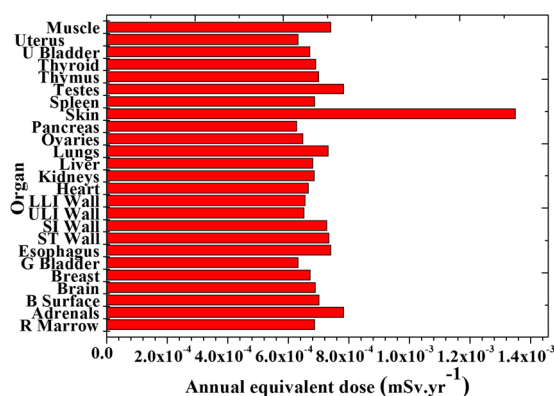


Figure 13. Total equivalent dose to different organs.

Discussion

Results show that some locations lead to over-exposure, for example, external hazard indices (H_{ex}) in some samples more than unity then it exceeds the upper limit of exposure. Also, radium equivalent activities (Ra_{eq}) in the same locations were higher than the exemption limits ($370 \text{ Bq}\cdot\text{kg}^{-1}$). While activity concentration indices (I) slightly exceed the permissible limits which met only $0.3 \text{ mSv}\cdot\text{yr}^{-1}$. Outdoor absorbed gamma dose rate (D_{out}) was ranged between 55.51 to 345.95 with an average of $186 \text{ nGy}\cdot\text{h}^{-1}$ which leads to effective outdoor gamma dose rate (E_{out}) ranged between 0.07 to 0.42 with an average of $0.23 \text{ mSv}\cdot\text{yr}^{-1}$ which represented more than 3 times higher than the world's average of $0.07 \text{ mSv}\cdot\text{yr}^{-1}$. The outdoor absorbed gamma dose rate was within the range as reported by UNSCEAR-2010 to Nile Delta region which met $20\text{--}400 \text{ nGy}\cdot\text{h}^{-1}$.

In general, it can be concluded that exposure in these areas was still within the permissible limits due to the little time of exposure as these areas are beaches that intended for hiking. Outdoor Excessive Lifetime Cancer Risk (ELCR_{out}) is found to be ranged between 0.24×10^{-3} – 1.49×10^{-3} with an average of 0.8×10^{-3} which is 2.8 times more than the upper limits 0.29×10^{-3} . It can be noticed that ELCR_{out} in all samples is greater than the upper recommended levels.

Annual equivalent dose due to average concentrations of all-natural radionuclides was ranged between 6.28×10^{-4} (received by the pancreas) and 1.35×10^{-3} mSvyr⁻¹ (received by skin). Average effective dose due to exposure to all radionuclides was 7.27×10^{-4} mSvyr⁻¹. It can be concluded that radiological hazard due to external exposure to different organs or tissues were within the international permissible values.

Material and Methods

About 30 samples were collected from north of Nile Delta near Rosetta beach parallel to the Mediterranean coast. This region is an open area, flat and nearly horizontal¹⁵. Samples were dried at 105 °C for 12 hours to completely remove residual moisture. About 500 g of each sample was mixed thoroughly, weighed and filled in a polyethylene jar with a screw cover and perfectly sealed with adhesive tapes to make them airtight. These containers were stored for one month at room temperature to allow secular equilibrium between ²²⁶Ra and its progenies to be achieved before gamma spectroscopy. For Gamma spectrometry a P-type coaxial HPGe detector, Canberra model No., CPVD 30–3020, shielded by 10 cm Pb thickness, 1 mm Cd and 1 mm Cu, with a relative efficiency of 30% and a resolution full width at half maximum (FWHM) of 1.9 keV at 1.33 MeV (with associated electronics) connected to multi-channel analyzer (MCA) and coupled with software program Genie 2000, was used. This detector is of high efficiency and has high resolution, and very low background, that it is important to get an estimate of the detection limits and the minimum detectable activity.

Efficiency calibration. The efficiency calibration must perform in the same geometry as used in the actual measurements. Efficiency calibration curve was done by using standard calibration sources (powder) produced by IAEA of ²³⁸U (RGU-1), with 400 ppm concentration, 1.78 density and activity 4.9 Bq/gm and ²³²Th (RGTh-1), with 800 ppm, 1.71 density and activity 3.26 Bq/gm were poured to the similar plastic jar up to the same height as sample. Pure silica was also poured to similar jar up to the same height as a sample. The energy calibration in 63.9–2614 keV was performed using the same standard sources. Determination of NORM was measured using different daughters that emit clear Gamma peaks of high intensity to confirm the attainment of radioactive secular equilibrium within the samples between ²²⁶Ra and its daughters. This was carried out by measuring ²²⁶Ra directly through the 186.2 keV and indirectly by measuring the ²¹⁴Bi (609.3, 1120.2 and 1764.5 keV) and ²¹⁴Pb (351.9 keV) photopeaks. ²³²Th was determined through ²²⁸Ac (911.2 keV) ²¹²Pb (238.6 keV after subtracting 241.2 value) and ²⁰⁸Tl (2614 keV) photopeaks, and estimation of ⁴⁰K through the 1460.8 keV photopeak. Samples and background were measured for about 6 hours for each.

Variation in uranium isotopic ratio ²³⁵U/²³⁸U. Identification of ²³⁵U concentration is difficult as its natural abundance concentration is low (only 0.72%) of natural uranium. The energy of 185.7 keV is the most intense gamma-ray line associated with the presence of ²³⁵U (57%). This is very close to the energy of 186.2 keV associated with the decay of ²²⁶Ra to ²²²Rn in ²³⁸U chain. Overlapping may occur during measurement. Due to the relatively lower branching ratios of 143.76 keV (10.96%), 163.33 keV (5.08%) and 205.31 keV (5.01%) energy transitions comparing to that of the 185.7 keV energy transition, they are not commonly used to determine ²³⁵U in black sand samples. Their counting rates due their expected counting rate would be below the detection limits ranges for the HPGe detector. So it is more practical to use the 185.7 keV energy transition to assess the ²³⁵U. Therefore, the concentration of ²³⁵U was calculated by subtracting the fraction of ²²⁶Ra using the following equation,^{19,20}

$${}^{235}\text{U} = \left(\frac{\left(\frac{\text{CR}_{187} / \varepsilon_{\text{peak}}}{M} - \text{AC}({}^{226}\text{Ra}) \times I_{\gamma}({}^{226}\text{Ra}) \right)}{I_{\gamma}({}^{235}\text{U})} \right) \quad (1)$$

where CR₁₈₇ is the count rate of the peak centered at 187 keV, ε_{peak} is the detector efficiency at that energy, M is the mass of the sample (kg), I_γ(²²⁶Ra) is the gamma-ray emission fraction for ²²⁶Ra, I_γ(²³⁵U) is the gamma-ray emission fraction for ²³⁵U, AC(²²⁶Ra) is the activity concentration of ²²⁶Ra in the sample (Bq.kg⁻¹) based on the average of the ²¹⁴Bi and ²¹⁴Pb analyses, and ²³⁵U is the concentration of ²³⁵U in the sample (Bq.kg⁻¹)²¹.

External and internal hazards calculations. *External Hazard Index (H_{ex}).* It is obtained from Ra_{eq} expression which indicates that the maximum allowable value (equal to unity) corresponds to the upper limit of Ra_{eq} (370 Bq.kg⁻¹). This value must be less than unity in order to minimize the radiation hazard, i.e., the radiation exposure must be limited to 1.0 mSv.yr⁻¹, then the external hazard index (H_{ex}) is given by the following equation:

$$H_{ex} = \frac{C_{Ra}}{370} + \frac{C_{Th}}{259} + \frac{C_K}{4810} \quad (2)$$

Where C_{Ra}, C_{Th} and C_K are the concentration in (Bq.kg⁻¹) of ²²⁶Ra²³², Th and ⁴⁰K respectively^{22,23}.

Radium Equivalent Activity (R_{eq}). External hazard index (H_{ex}) can be calculated by another method as expression called radium equivalent activity R_{eq} for comparing the specific activity of materials containing different amounts of ^{226}Ra , ^{232}Th and ^{40}K . It is based on the fact that 370 (Bqkg^{-1}) of ^{226}Ra , 259 (Bqkg^{-1}) of ^{232}Th and 4810 (Bqkg^{-1}) of ^{40}K , produce the same γ -ray dose equivalent. It is defined by the following expression^{17,24}:

$$R_{eq} = C_{Ra} + 1.43C_{Th} + 0.077C_K \quad (3)$$

Activity Concentration Index (I). The activity concentration index should be used for identifying materials which might be of concern. It is used to present investigation levels in the form of an activity concentration index, (I), or shortly, gamma index (I), and it is defined as follows²⁵:

$$I = \frac{C_{Ra}}{300} + \frac{C_{Th}}{200} + \frac{C_K}{3000} \quad (4)$$

The maximum value for activity concentration index is 2 ($I \leq 2$) to meet 0.3 mSvyr^{-1} dose criterion and $I \leq 6$ to meet 1 mSvyr^{-1} ^{26,27}.

Alpha Index (I_α):

The alpha index is used to assess the excess alpha radiation internal exposure caused by inhalation of naturally occurring radionuclides. When the activity concentration of ^{226}Ra exceeds a value of 200 Bqkg^{-1} , it is possible that the radon exhaled from this material met a concentration of 200 Bqm^{-3} . Many countries of the world suggested the exemption level and upper level of ^{226}Ra activity of 100 Bqkg^{-1} and 200 Bqkg^{-1} respectively²⁸.

Outdoor Absorbed Gamma Dose Rate (D_{out}):

The outdoor absorbed gamma dose rate (D_{out}) at 1 meter above the ground surface due to uniformly distributed natural radionuclides can be calculated as follows^{29,30}:

$$D_{out} = 0.43 C_{Ra} + 0.666 C_{Th} + 0.047 C_K (\text{nGy} \cdot \text{h}^{-1}) \quad (5)$$

Annual Outdoor Effective Dose (E_{out}):

Annual outdoor effective dose (E_{out}) can be calculated from the dose rate (D_{out}), about 20% of 8760 hours in a year can be considered as time of stay in the outdoor and for converting absorbed dose in air to effective dose a factor of 0.7 SvGy^{-1} was used, and can be calculated as follow³¹:

$$E_{out} \left(\frac{\text{mSv}}{\text{y}} \right) = D_{out} \left(\frac{\text{nGy}}{\text{h}} \right) \times 0.7 \times 8766 \times 0.2 \times 10^{-6} \quad (6)$$

Excessive Lifetime Cancer Risk (ELCR):

Outdoor Excess Lifetime Cancer Risk ($ELCR_{out}$) is calculated from outdoor annual effective dose according to the following equation¹⁸:

$$ELCR_{out} = E_{out} \times LE \times RF \quad (7)$$

Where LE represents the life expectancy (70 years) and RF represents the fatal risk factor per Sievert (Sv^{-1}). ICRP-60³² uses RF values of 0.05 for the public in case of stochastic effects.

External Equivalent and Effective Dose to Organs or Tissues:

Organ doses due to external exposure were determined by Eckerman and Ryman (DFEXT-code)³³. The coefficients in this software represent the dose per unit integrated exposure or the dose rate per unit concentration ($\text{Sv m}^3/\text{sec Bq}$). So, activity concentrations were transformed from Bqkg^{-1} into Bqm^{-3} .

Where the summation extends over the organs/tissues with explicit W_t , W_{rem} is the weighting factors for the remainder (0.2), and h_{rem} is the committed dose equivalent per unit integrated exposure for the remainder tissues. h_{rem} is given as: $h_{rem} = 1/5 \sum h_t$.

From these coefficients, equivalent dose (H_t) to any organ from any radionuclide can be calculated as follows:

$$H_T = C \times T \times 3600 (\text{sec/hr}) \times h_t (\text{Sv}) \quad (8)$$

While the effective dose (E) can be calculated as follows:

$$E = C \times T \times 3600 \times e (\text{Sv}) \quad (9)$$

Where:

1. $-h_t$ is the equivalent dose in tissue (t) per unit integrated exposure ($\text{Sv m}^3/\text{sec Bq}$),
2. $-e$ is the effective dose per unit integrated exposure = $\sum W_t h_t$, using W_t from ICRP-60,
3. $-C$ is the activity concentration in black sand (Bq/m^3),
4. $-T$ is the exposure time ($8766 \times 0.2 \text{ h/year}$).

References

- Vasconcelos, D. C. *et al.* Modeling Natural Radioactivity in Sand Beaches of Guarapari, Espirito State, Brazil. *World. Journal of Nuclear Science and Technology*. **3**, 65–71 (2013).
- Danilo C. Vasconcelos *et al.* Determination of Uranium and Thorium Activity Concentrations Using Activation Analysis Beach Sands from Extreme South Bahia, Brazil”, International Nuclear Atlantic Conference 27 September – 2 October, Rio De Janeiro, Brazil (2009).
- Sarojini V. Baseline Assessment of Dose due to Natural Radionuclides in Soils of Coastal Regions of Kanyakumari District in Tami Nadu, India. *IOSR J. of Environ. Sci. Toxicology and Food Tech.* **8**(9), III, 1–4(2014).
- Nada, A. *et al.* Correlation between Radionuclides Associated with Zircon and Monazite in Beach Sand of Rosetta, Egypt. *J. Radiation. Nucl. Ch.* **291**, 601–610 (2012).
- Filippidis, Anestis *et al.* Mineral, Chemical and Radiological Investigation of A black Sand at Touzla Cape, Near Thessaloniki, Greece. *Environmental Geochemistry and Health*. **19**, 83–88 (1997).
- Shetty, P. K., Narayana, Y. & Rajashekara, K. M. Depth Profile Study of Natural Radionuclides in the Environment of Coastal Kerala. *J. Radioanal. Nucl. Ch.* **290**, 159–163 (2011).
- Santos, I. R., Burnett, W. C. & Godoy, J. M. Radionuclides as Tracers of Coastal Processes in Brazil: Review, Synthesis and Perspectives. *Brazilian Journal of Oceanography*. **56**(2), 115–131 (2008).
- Vassas, C., Pourcelot, L. *et al.* Mechanisms of Enrichment of Natural Radioactivity Along the Beaches of the Camargue, France. *J. Environ. Radioactiv.* **91**, 146–159 (2006).
- Argyrios Papadopoulos, Antonios Koroneos, Georgios Christofides & Stylianos Stoulos. Natural Radioactivity Distribution and Gamma Radiation exposure of Beach sands Close to Maronia and Samthraki Plutons, NE Greece. *Geological Balcanica*. **43**, 1–3, Sofia, p. 99–107(2014).
- Papadopoulos, Argyrios *et al.* Natural Radioactivity and Radiation Index of the Major Granitic Plutons in Greece. *Journal of Environmental Radioactivity*. **124**, 227–238 (2013).
- Papadopoulos, Argyrios, Christofides, Georgios, Koroneos, Antonios & Stoulos, Stylianos Natural Radioactivity Distribution and Gamma Radiation Exposure of Beach Sands from Sithonia Peninsula, Cent. Eur. *J. Geosci.* **6**(2), 229–242 (2014).
- Harb, s Natural Radioactivity and External Gamma Radiation Exposure at Coastal Red Sea in Egypt. *Radiat. Prot. Dosim.* **130**, 376–384 (2008).
- Tsuey-Lin, T., Chi-Chang, L., Chun-Yu, C., Hwa-Jon, W. & Lee-Chung, M. The Effects of Physico-Chemical Properties on Natural Radioactivity Levels, Associated Dose Rate and Evaluation of Radiation Hazard in The Soil of Taiwan Using Statistical Analysis. *Journal of Radioanal. And Nucl. Ch.* **288**(3), 927–936 (2011).
- Jabbar, A. *et al.* Measurement of Soil Radioactivity Levels and Radiation Hazard Assessment in Mid Rechna Interfluvial Region, Pakistan. *Journal of Radioanalytical and Nuclear Chemistry*. **283**, 371–378 (2010).
- Attiah A.M. Environmental Assessment of Rosetta Area, Mediterranean Sea Coast – Egypt, MS.D. Thesis. Fac. Sci., Zagazig University. Egypt (2011).
- Mohanty, A. K., Sengupta, D., Das, S. K., Vijayan, V. & Saha, S. K. Natural Radioactivity in the Newly Discovered High Background Radiation Area on the Eastern Coast of Orissa, India. *Radiation Measurements*. **38**, 153–165 (2004).
- UNSCEAR. Sources and Effects of Ionizing Radiation United Nations Scientific Committee on the Effects of Atomic Radiation. United Nations Publication, New York, USA (2010).
- Shittu, H. O. *et al.* Determination of the Radiological Risk Associated with Naturally Occurring Radioactive Materials (NORM) at Selected Quarry Sites in Abuja, FCT, Nigeria: Using Gamma-Ray Spectroscopy. *Physics Journal*. **1**(2), 71–78 (2015).
- Wahl, W. Radionuclide Handbook for Laboratory Workers in Spectrometry, Radiation Protection and Medicine”, Germany: ISUS (2007).
- NNDC. National Nuclear Data Center <http://www.nndc.bnl.gov> [Updated November 2016].
- Powell, B. A. *et al.* Elevated concentrations of primordial radionuclides insediments from the Reedy River and surrounding creeks in Simpsonville, South Carolina. *Journal of Environmental Radioactivity*. **94**, 121–128 (2007).
- Eissa, M. F., Mostafa, R. M., Shahin, F., Hassan, K. F. & Saleh, Z. A. Natural Radioactivity of Some Egyptian Building Materials. *Int. J. Low Radiation*. **5**(1), 1–8 (2008).
- Attia, T. E., Shendi, E. H., & Shehata, M. A. Assessment of Natural and Artificial Radioactivity Levels and Radiation Hazards and their Relation to Heavy Metals in the Industrial Area of Port Said City, Egypt. *J Earth Sci Clim Change*. 1–11(2014).
- Xhixha, G., *et al.* First Characterization of Natural Radioactivity in Building Materials Manufactured in Albania. *Radiation Protection Dosimetry*. 1–7 (2013).
- Todorovic, N. *et al.* Natural Radioactivity in Raw Materials Used in Building Industry in Serbia. *Int. J. Environ. Sci. Technol.* **12**, 705–716 (2015).
- European Commission (EUC). *Radiological Protection Principles Concerning the Natural Radioactivity of Building Materials*, European Commission, *Radiation Protection* **112**, 4–16 (1999).
- Nisha, Sharma, Singh, Jaspal, Esakki, S. Chinna & Tripathi, R. M. A Study of The Natural Radioactivity and Radon Exhalation Rate in Some Cements Used in India and Its Radiological Significance. *Journal of Radiation Research and Applied Sciences*. **9**, 47–56 (2016).
- Raghu, Y., Harikrishnan, N., Chandrasekaran, A. & Ravisanakar, R. Assessment of Natural Radioactivity and Associated Radiation Hazards in Some Building Materials Used in Kilpenathur, Tiruvannamalai Dist, Tamilnadu, India. *African Journal of Basic & Applied Sciences*. **7**(1), 16–25 (2015).
- Shams, A. M., Issa & Alaseri, S. M. Determination of Natural Radioactivity and Associated Radiological Risk in Building Materials Used in Tabuk Area, Saudi Arabia, Inter. *J. of Advanced and Technology*. **82**(5), 45–62 (2015).
- Abd El Wahab, M. & El Nahas, H. A. Radionuclides Measurements and Mineralogical Studies on Beach Sands, East Rosetta Estuary, Egypt. *Chin.J. Geochem.* **32**, 146–156 (2013).
- Masila, Xolani Radioactive Nuclides in Phosphogypsum from the Lowveld Region of South Africa. *S. Afr. J. Sci.* **112**(1/2), 1–5 (2016).
- ICRP. International Commission on Radiological Protection, “The Recommendations of the Commission,” ICRP Publication 60, Annals of the ICRP, 21(1–3) (1991a) (Pergamon Press, New York). **3**, 295–302 (1990).
- Eckerman, K. F. & Ryman, J. C. External Exposure to Radionuclides in Air, Water, and Soil. Federal Guidance Report No. 12, EPA Report 402-R-93–081 (Washington, DC) (1993).

Author Contributions

Fawzia Mubarak, M. Fayeze-Hassan, N. A. Mansour, Talaat Salah Ahmed and Abdallah Ali wrote the main manuscript text and Abdallah Ali prepared Fig. 1–13.

Additional Information

Competing Interests: The authors declare that they have no competing interests.

Publisher's note: Springer Nature remains neutral with regard to jurisdictional claims in published maps and institutional affiliations.



Open Access This article is licensed under a Creative Commons Attribution 4.0 International License, which permits use, sharing, adaptation, distribution and reproduction in any medium or format, as long as you give appropriate credit to the original author(s) and the source, provide a link to the Creative Commons license, and indicate if changes were made. The images or other third party material in this article are included in the article's Creative Commons license, unless indicated otherwise in a credit line to the material. If material is not included in the article's Creative Commons license and your intended use is not permitted by statutory regulation or exceeds the permitted use, you will need to obtain permission directly from the copyright holder. To view a copy of this license, visit <http://creativecommons.org/licenses/by/4.0/>.

© The Author(s) 2017